Deterministic generation of single B centers in hBN by one-to-one conversion from UV centers

Andrés Núñez Marcos, Christophe Arnold, Julien Barjon, Stéphanie Buil, Jean-Pierre Hermier, Aymeric Delteil *Université Paris-Saclay, UVSQ, CNRS, GEMaC, 78000, Versailles, France.*(Dated: November 5, 2025)

Among the variety of quantum emitters in hexagonal boron nitride (hBN), blue-emitting color centers, or B centers, have gathered a particular interest owing to their excellent quantum optical properties. Moreover, the fact that they can be locally activated by an electron beam makes them suitable for top-down integration in photonic devices. However, in the absence of a real-time monitoring technique sensitive to individual emitters, the activation process is stochastic in the number of emitters, and its mechanism is under debate. Here, we implement an in-situ cathodoluminescence monitoring setup capable of detecting individual quantum emitters in the blue and ultraviolet (UV) range. We demonstrate that the activation of individual B centers is spatially and temporally correlated with the deactivation of individual UV centers emitting at 4.1 eV, which are ubiquitous in hBN. We then make use of the ability to detect individual B center activation events to demonstrate the controlled creation of an array with only one emitter per irradiation site. Additionally, we demonstrate a symmetric technique for heralded selective deactivation of individual emitters. Our results provide insights into the microscopic structure and activation mechanism of B centers, as well as versatile techniques for their deterministic integration.

I. INTRODUCTION

Optically active point defects in crystals, commonly referred to as color centers, are of great significance in quantum information science due to their ability to act as singlephoton emitters (SPEs) and their compatibility with nanostructures and devices [1]. A well-known example is the nitrogen-vacancy (NV) center in diamond, which forms the foundation of many emerging quantum network architectures [2]. More recently, the discovery of color centers in van der Waals materials has opened new avenues for integration and applications in quantum technologies [3], with hexagonal boron nitride (hBN) being a particularly promising host. This wide-bandgap semiconductor can indeed integrate high quality SPEs [4, 5]. A specific class of hBN emitters is distinguished by its remarkable quantum optical properties. The so-called B centers reproducibly emit at 436 nm and exhibit photon indistinguishability at low temperature [6, 7]. They are not found natively but can be locally activated by a focused electron beam [8-10], which is an asset for the controlled integration in photonic devices [11, 12]. However, the activation mechanism is still debated and yields an unpredictable number of SPEs, due to the lack of a technique for heralding the successful creation of single emitters.

The microscopic structure of the B centers is still under debate. Some important clues have been however identified. In particular, the B center activation is efficient only in crystals exhibiting the optical signature of UV centers [10]. These UV color centers emitting at 4.1 eV are commonly found in carbon-rich hBN [13–18] and are attributed to in-plane carbon dimers (C_BC_N) [19–21]. Cathodoluminescence (CL) has been shown to allow for real-time monitoring of the emitter population dynamics under electron irradiation, allowing to study the kinetics of B center creation [22] and to observe the concurrence of a decrease in the population of UV centers [23], albeit with a different timescale. These studies have been performed on ensembles and at room temperature, therefore the possible relation between UV and B centers remains unclear. Moreover, the activation and deactivation of presumably individual

B centers has been observed [8, 24], but without insights about the mechanism of such dynamics and the relation to individual UV centers. Concerning the microscopic structure of B centers, several candidates have been proposed, such as a split nitrogen interstitial [25, 26], a carbon tetramer [27, 28], and a vertical carbon dimer [25]. The latter hypothesis seems to have been confirmed very recently by a bundle of consistent clues obtained with combined STEM/HAADF and CL measurements [24].

Here, we investigate the activation and deactivation of individual B and UV centers upon irradiation by an electron beam, through a specifically designed CL detection setup based on avalanche photodiodes (APDs), which makes the in-situ monitoring sensitive to the single emitter level in both wavelength ranges. We show that individual creation events of B centers are accompanied by a simultaneous abrupt deactivation of a UV center, correlated both in time and space. This suggests a one-to-one transformation of UV to B centers. The conversion is partially reversible, as the opposite process is also observed. At long times, B centers stabilize into a steady state population, as demonstrated in prior work [22, 23]. In a second step, we make use of the in-situ monitoring signal as a marker that heralds successful creation of individual emitters. We demonstrate a small array of emitters with strongly sub-Poissonian statistics of emitter numbers, as confirmed with the measurement of their second-order correlation function. We then show that accidental double creations can be corrected for using heralded photobleaching, further reducing the variations in emitter numbers. In a conclusive discussion, we tentatively provide a mechanism for supporting the observed UV-blue conversion, consistent with the vertical carbon dimer hypothesis for the microscopic structure of B centers.

II. INTERCONVERSION OF UV AND B CENTERS

The experimental setup which allows for in-situ monitoring of the activation and deactivation of individual color centers in the UV and blue spectral range is presented in Figure 1a.

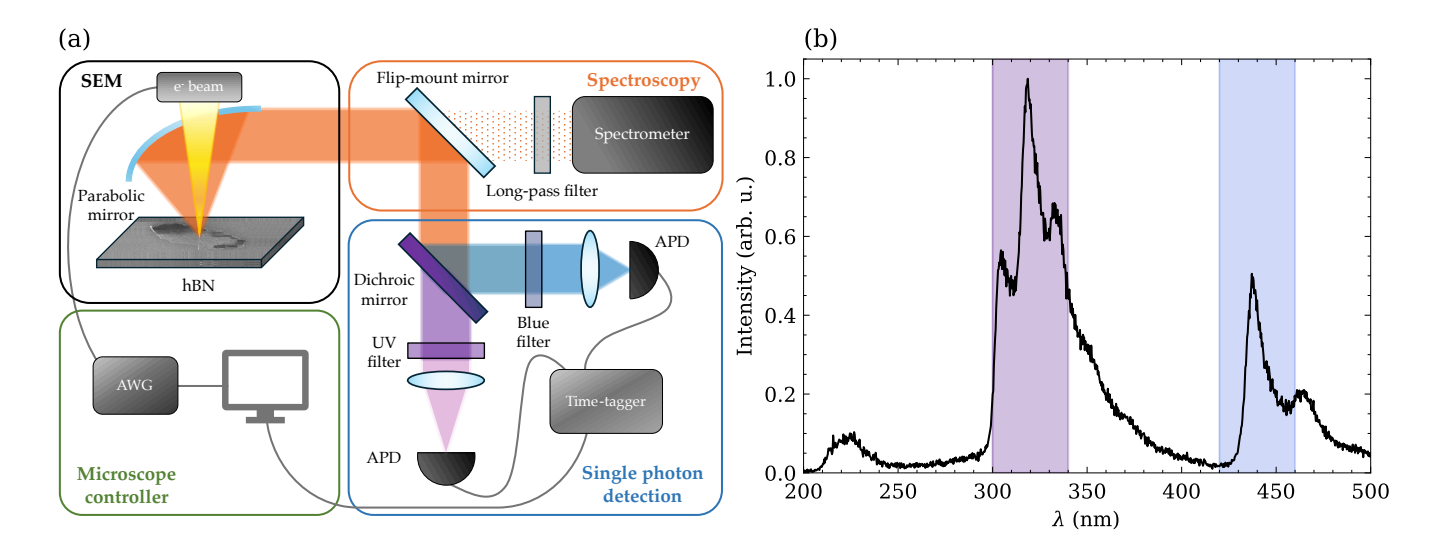


FIG. 1. (a) Scheme of the experimental setup. AWG: arbitrary waveform generator. (b) Black line: CL spectrum of a hBN sample containing UV and blue emitters. Violet shading: UV filter passband. Blue shading: Blue filter passband. The visible-range part of the spectrum was taken with a UV filter to suppress second-order refraction of the exciton emission.

The sample is placed inside a scanning electron microscope (SEM), where a holed parabolic mirror is positioned above the sample to collect the emitted photons outside the microscope. A spectrometer is placed at the output port of the SEM. Figure 1b shows the CL spectrum of a hBN crystal under electron irradiation. Three recognizable features can be observed. The exciton emission is visible at about 215 nm; the three equally spaced peaks in the 300-350 nm range are the signature of the UV emitter C_BC_N with a zero-phonon line at 305 nm and its phonon replica; the peaks at 440 nm and 465 nm originate respectively from the B center zero-phonon line and optical phonon replica [13, 21, 29]. Using a flip-mount mirror, we can channel the emission to a single-photon detection system. The emitted light is then separated into two frequency bands, UV and blue regions respectively, using a dichroic mirror and bandpass filters. The bandwidth of both detection channels is depicted by the shaded areas on Fig. 1b. Both signals are simultaneously detected by APDs. This setup allows to be sensitive to the CL signal associated with individual UV and B centers.

We first select a hBN crystal of thickness 145 nm, where the density of UV centers is low enough to spatially resolve individual emitters (see Methods for sample preparation). Figure 2a shows a series of four consecutive CL scans of the same region of space. The scanning time is about ten minutes, and the scan direction is from left to right, then from top to bottom. Both UV and blue channels are recorded in parallel, simultaneously. The top (bottom) panels plots the UV (blue) band signal. We refer to these successive maps as scan 1 to 4. In both spectral ranges, various point emitters can be observed. In addition, some emitters of both species either appear or disappear during scans. To ease the discussion, we select five representative sites, depicted by circles in both spectral regions and labeled by letters A to E. The circle colors indicate that the emitters are active (green circles), in-

active (red circles) or switching (two-colored circles). In the UV maps, sites A and B indicate UV emitters that are active during scans 1 and 2 (upper panel), while no blue emitter is observed at these same sites (lower panel). In scan 3, the UV emitters located sites A and B are deactivated, which shows up as interrupted spots with CL signal only in the upper part. Simultaneously, signal appears in the blue range at the same locations. The switching appears instantaneous at the timescale of the integration time per pixel (100 ms), as the blue signal appears at the same pixels where the UV signal disappears. In scan 4, no UV emitter is visible in sites A and B, while blue emitters now appear as full spots. Sites C and D exhibit the inverse process along the four scans, with blue emitters initially present in scan 1, switching to UV during scan 2, and staying visible as UV emitters in the two following scans. Finally, site E undergoes a bidirectional process, with an initial switching from UV to blue during scan 1, staying in the blue state during scans 2 and 3, and switching back to UV during scan 4. Other similar events can be observed on these CL scans, as well as all other scans we performed. We illustrate this further by showing consecutive scans of two emitters on Figure 2b and c. Both emitters exhibit multiple switching events between the UV and the blue state while the electron beam is passing over them. Additional examples of consecutive scans are shown in the Supporting Information section S1. Overall, our observations can be summarized as follows.

- (1) The activation of B centers is observed simultaneously with the deactivation of UV centers.
- (2) The reverse process is also observed, demonstrating that the conversion is at least partially reversible.
- (3) The conversion is faster than our integration time per pixel (100 ms).
- (4) The switching occurs exactly under the electron beam, as testified by truncated CL spots, with the signal appearing or disappearing at the emitter position. This can be observed

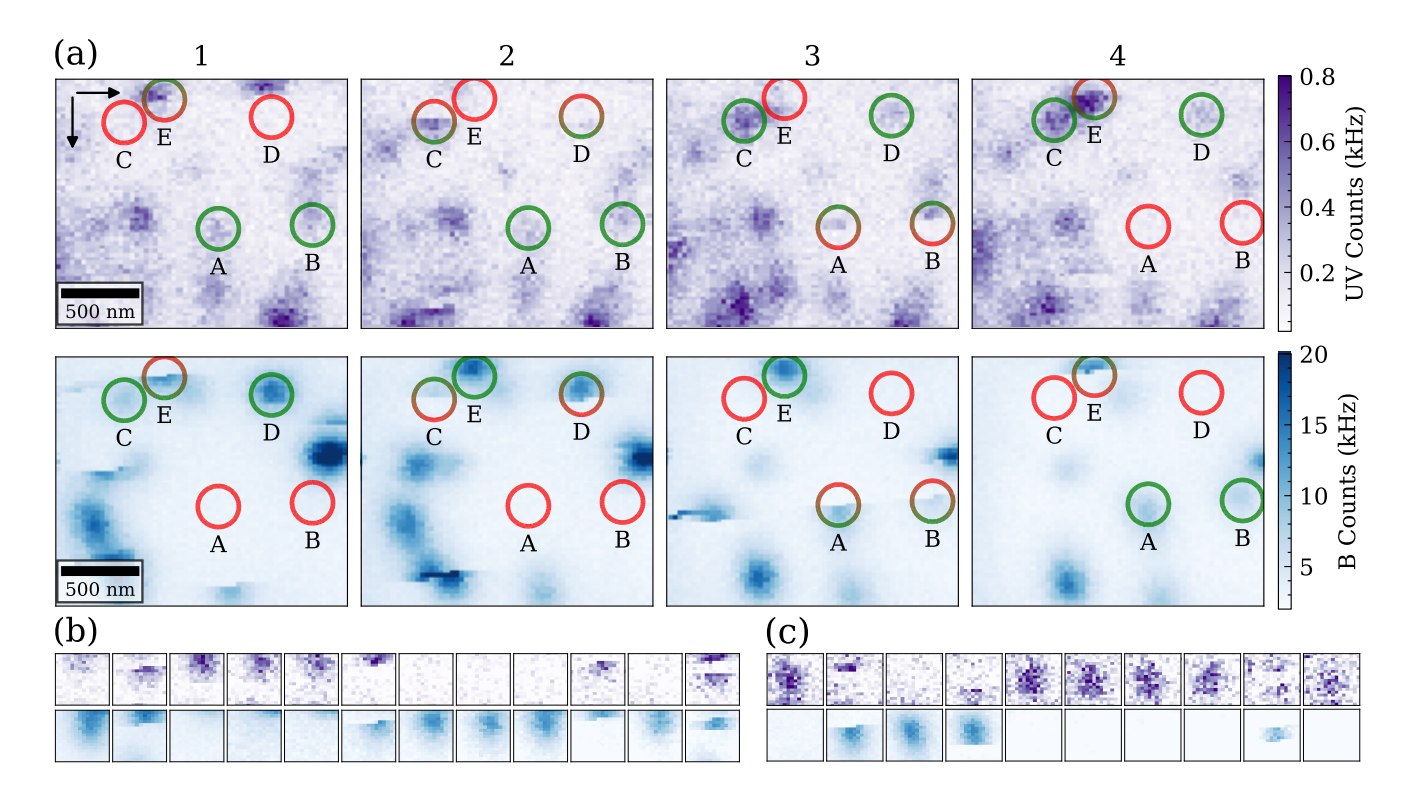


FIG. 2. (a) Series of CL bandpass images of color centers in a hBN flake of thickness 145 nm with a current intensity of I = 0.024 nA. The top row shows the signal measured in the UV detection channel and the bottom row displays the signal measured in the blue detection channel. The scale bar indicates 500 nm. The circles labeled A to E indicate the state of five emitters: a red circle indicates the color center is off, a green circle indicates the emitter is on, and a two-colored circle indicates that an activation or deactivation is taking place. The states of the blue and UV emitters occupying these five positions are anticorrelated. (b) and (c) Consecutive CL scans of two fixed emitters in the UV (top) and blue (bottom) spectral range, showing switching between the two states.

as incomplete lines of bright pixels switching while the electron beam is scanning over the SPE. This implies that the process is driven locally by the electron beam, and not by indirect consequences of the irradiation process, such as charge accumulation or heat. This also demonstrates that, in samples with high concentration of UV centers, the resolution of the B center creation is solely given by the SEM resolution.

(5) Essentially all occurrences where a single UV center disappears while scanning are associated with the appearance of a B center. This suggests that the conversion to B center is the main – if not the only – decay process of the UV center under electron irradiation. Other mechanisms were proposed [30] but are likely slower or less probable, at least in our range of irradiation parameters.

The ability to observe the activation of individual emitters opens the way to the deterministic fabrication of a single one, which is what we investigate in the next section.

III. HERALDED ACTIVATION OF B CENTERS

We now select a flake with a higher density of UV centers, such that conversion can occur at any location. Such flakes exhibit a large UV signal, similar as the spectrum shown Fig. 1b. We continuously irradiate the crystal at a fixed posi-

tion, while recording the signal of B centers with the APD. Figure 3 shows a representative example of the intensity trace measured during 80 s. Discrete increases of the signal can be observed, showing that individual creation events can be unambiguously identified. The signal associated with the creation of individual emitters is about 10³ to 10⁴ counts per second. A few downward steps are also visible, associated with

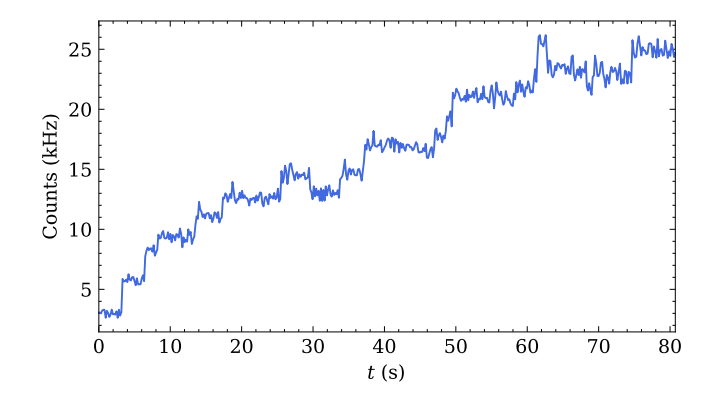
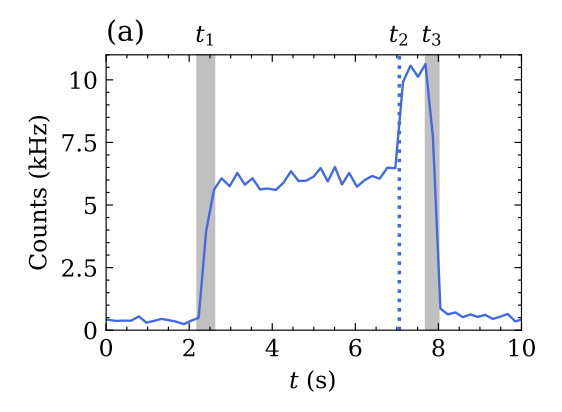
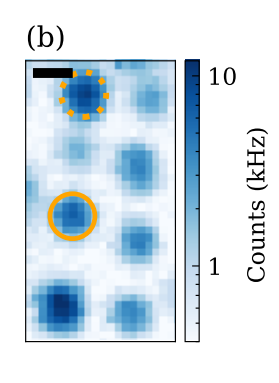


FIG. 3. Representative CL timetrace measured by the blue detection channel during a continuous irradiation of a fixed location on a 130 nm flake with I = 0.021 nA.





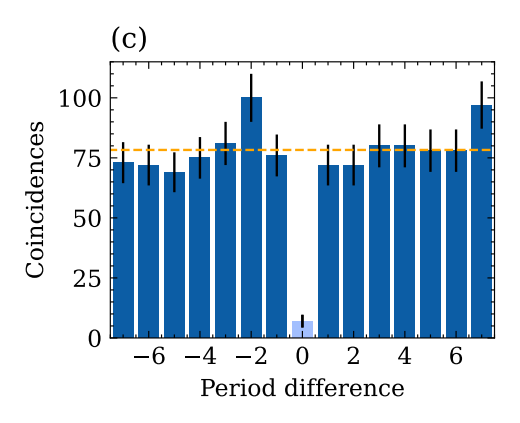


FIG. 4. (a) CL intensity trace of the blue detection channel: at t_1 the e^- beam is turned on, at t_2 a single B center is generated and at t_3 the e^- beam is turned off. (b) PL map of a 4×2 array of B centers activated in a 50 nm thick flake, with a distance of 1 μ m between irradiation sites. The scale bar indicates 500 nm. The orange circle indicates the individual B center characterized in Fig. 4c and the dotted orange circle denotes the irradiation site characterized in Fig. 5. (c) $g^{(2)}(\tau)$ measured for the B center circled in orange in the PL map, with $g^{(2)}(0) = 0.09 \pm 0.03$. Orange dashed line: Classical limit.

deactivations as observed in the previous section. However, the overall trend is a global increase of the number of emitters, consistently with prior work on large ensembles [22, 23]. This suggests that the blue emitters are stabilized under continuous irradiation. Each upward step constitutes a signal heralding the success of individual B center activation.

We illustrate the potential use of the individual activation monitoring by realizing an array of single emitters as a proof of principle. We irradiate at eight chosen locations while monitoring the signal, and we interrupt the irradiation after the first upward step is observed. An example of real-time signal is shown Figure 4a. The protocol is the following:

- (1) We switch on the electron beam at t_1 , from where a background luminescence signal of about 5 kHz is observed.
 - (2) At time t_2 , an upward step is observed.
- (3) Shortly after, the electron beam is switched off manually, at time t_3 , using the built-in blanking system of the SEM.
- (4) We repeat this process at eight different locations in a 4×2 array, with 1 μ m distance between sites.

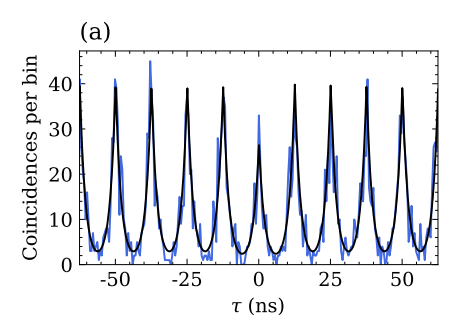
The sample is subsequently characterized in photoluminescence (PL) at room temperature, in a confocal microscope. A pulsed laser emitting at 405 nm is used to excite the emitters. Figure 4b shows a PL confocal map of the sample. Eight luminescent spots are visible. The slight misalignment of the spot array originates from hysteresis of the piezoelectric positioner used to define the irradiation sites. The emitters are characterized in a Hanbury Brown and Twiss setup to estimate the number of emitters. A value of $g^{(2)}(0) < 0.5$ is attributed to a single emitter. An example of $g^{(2)}(0)$ is shown on Figure 4c, corresponding to the circled spot on Figure 4b. Among the eight sites, seven are single emitters, and one, indicated by the dotted circle on Figure 4b, has a higher $g^{(2)}(0)$. The latter corresponds to an event where two steps were observed before the electron beam was blanked. A workaround for such cases is proposed in the next section.

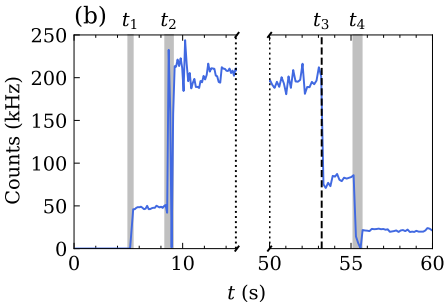
This proof of principle demonstrates the ability to control the number of activated color centers. Without the active feedback developed in this work using in-situ CL monitoring, a Poisson distribution of the emitter numbers would have been obtained, yielding single centers in at most 37 % of the irradiated spots (vs. 87 % in the present case). In the following, we demonstrate an additional step to narrow down the distribution further in case of undesired double activation, as for one of the eight sites here.

IV. CONTROLLED DEACTIVATION BY PHOTOBLEACHING

A symmetrical approach to the activation protocol can be used for selective deactivation. B centers are very stable under laser illumination at low to moderate powers, up to about 1-2 mW, as testified by week-long measurements in PL and resonant excitation [6, 7]. This power regime is therefore considered as "safe" for the emitters. However, the B centers can photobleach when exposed to a continuous-wave (cw) PL laser at high power ($\gtrsim 4 \text{ mW}$) during a few tens to hundreds of seconds [31]. We demonstrate how this phenomenon can be used to selectively remove an emitter from an irradiation site where two emitters are present, using cw laser drive in the high-power, "unstable" regime. We base our approach on realtime monitoring of the PL during laser illumination, in analogy with the activation case. To illustrate this technique, we consider the site of the array shown on Figure 4b (dotted orange circle) that exhibits $g^{(2)} > 0.5$. Figure 5a shows the $g^{(2)}$ of this site before selective bleaching, measured in the pulsed regime. The center peak has a value of $g^{(2)}(0) = 0.67 \pm 0.05$. We apply the selective photobleaching technique while monitoring the PL signal, shown on Figure 5b. The process is as

- (1) The cw laser is switched on at time t_1 , with a power of 0.75 mW, in the safe power regime. The count rate is about 50 kHz.
- (2) The power is abruptly raised to 7.5 mW, in the "unstable" regime, by removing a neutral density filter at time t_2 . The count rate increases to 200 kHz, above saturation.





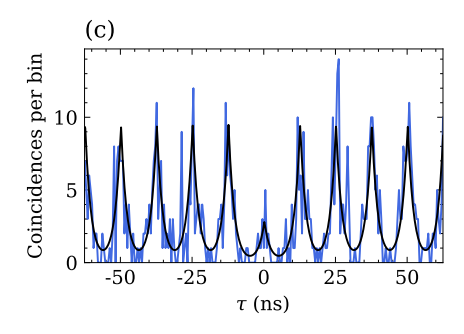


FIG. 5. (a) Blue line: $g^{(2)}(\tau)$ measured from the brightest B-center in the PL map (dashed orange circle in Figure 4b). Black line: Fit to the data, where $g^{(2)}(0) = 0.67 \pm 0.05$ (b) PL timetrace measured during the selective photobleaching procress; t_1 : the laser is turned on with a neutral density filter, yielding a 750 μ W power; t_2 : the absorption filter is removed, so that the excitation power increases to 7.5 mW; t_3 : a B-center has been deactivated; t_4 : the absorption filter is inserted back. (c) Blue line: $g^{(2)}(\tau)$ measured at the same position after the photobleaching process. Black line: fit to the data, providing $g^{(2)}(0) = 0.29 \pm 0.11$.

- (3) At time t_3 , a downward step is observed, heralding bleaching of an emitter. The count rate is about 80 kHz.
- (4) Shortly after, we put back the neutral density filter at time t_4 to return in the safe power regime. The count rate is then about 20 kHz.

To verify that the remaining signal comes from a single emitter, we measure the $g^{(2)}$ function again. The result is shown on Figure 5c. The value of $g^{(2)}(0) = 0.29 \pm 0.11$ testifies that only one emitter is now active on the site. Further examples of controlled bleaching are shown in the Supporting Information section S2, to demonstrate the reproducibility of the method. We note that bleaching occurs after a few tens of seconds, making it straightforward to isolate a single bleaching event. The combined monitoring of SPE activation using CL, and deactivation using PL, allows us to reach 100 % success for the creation of single B centers.

V. DISCUSSION ABOUT THE CONVERSION MECHANISM

The ability to simultaneously resolve UV and B centers at the individual level has allowed us to observe electron-beam induced direct interconversion between these two species. Such events can shed additional light on the microscopic structure of both defects. Recent experimental studies identify the UV defect as a horizontal carbon dimer (C_BC_N) [21] (Fig. 6a) and the B center as a vertical carbon dimer in a split interstitial configuration (Fig. 6b), either at a boron site $(2C_i)_R$ or at a nitrogen site $(2C_i)_N$ [24]. In the light of these conclusions, our results can be interpreted as the observation of electron-beam induced modification of a carbon complex, and provides additional credit to both identifications. Indeed, no other pair of candidates for either UV or B centers can be easily linked together among the plausible candidates proposed in the literature [19–21, 24, 26, 27, 32]. However, a subtlety stands in the fact that the vertical dimer structure replaces only one atom of the hBN lattice, while the horizontal dimer occupies two atomic sites (Fig. 6). Therefore, the electron-beam activation process of the B center is not a simple 90° rotation

of the in-plane carbon dimer, and necessarily involves an additional species.

To account for the additional atom in the B center structure as compared with the UV center, we propose the following scenario, where a vacancy is created when switching from the horizontal to the vertical configuration of the carbon doublet.

$$C_B C_N \rightleftharpoons (2C_i)_N + V_B \tag{1}$$

where we have supposed that the B center is at the nitrogen

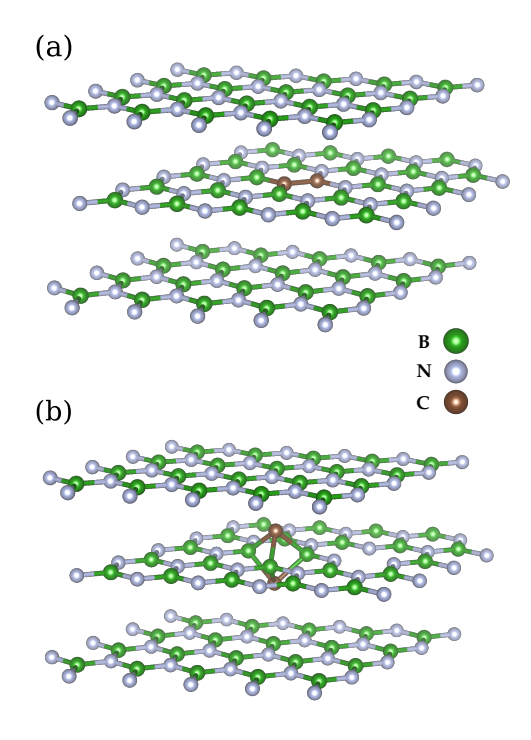


FIG. 6. Possible microscopic models for the studied defects. (a) Inplane carbon dimer C_BC_N for the UV center and (b) carbon dimer in split interstitial configuration $(2C_i)_N$ for the B center, with a leftover vacancy after conversion.

site, *i.e.* $(2C_i)_N$, without loss of generality since the boron site counterpart can be obtained by permuting N and B. The conversion is reversible according to our observations. However, the vacancy is known to be mobile [33, 34]. Upon diffusion (which can be induced by the electron beam [34]), the vacancy migration prevents backwards conversion and locks the defect to the $(2C_i)_N$ state, consistently with the observed stability of the B centers at long times.

Another possible scenario would involve the recombination of a boron interstitial with the UV center to form a B center: $C_BC_N + B_i \rightleftharpoons (2C_i)_N$. We do not retain this scenario since it would require the unlikely presence of interstitials at a high concentration so to allow conversion of UV centers with a high yield. Additionally, since boron interstitials are mobile in hBN [33] and the UV-B conversion is reversible, the long-time stable state upon migration of the interstitial is the UV center C_RC_N, which is inconsistent with observations. Therefore, we believe that the first scenario describing the dissociation of the in-plane carbon dimer into a vertical dimer and a vacancy, followed by migration of the vacancy, explains both the partial reversibility at short times, and the long-time stability. Furthermore, due to the sizably higher mobility of the boron vacancy as compared with the nitrogen vacancy [33, 35], we favor the choice of $(2C_i)_N + V_B$ rather than $(2C_i)_B + V_N$ as the final product of the electron-beam-induced conversion.

VI. CONCLUSION

We have observed electron-beam induced interconversion between individual UV centers and B centers, appearing as abrupt anticorrelated activation or deactivation events of the point defect emission on simultaneously recorded CL scans. This electron-induced switching between these two widely studied color centers shed new light onto their long debated microscopic structure and their mutual relation, consolidating the recent hypothesis that B centers are vertical carbon dimers. Our results provide a direct explanation for the well-known fact that B centers can only be activated in hBN crystals exhibiting the 4.1 eV spectral signature of the UV centers, and suggests a possible activation scenario, where the electron

beam would modify the dimer orientation, which would then be made stable by evacuating the leftover vacancy.

In addition, the ability to observe individual activation events has allowed us to make use of the CL signal as a marker heralding the successful activation of single B centers. We illustrated this by generating an array of eight sites with a strongly sub-Poissonnian distribution of the SPE numbers. The rare and undesired double creations can be fixed by selective photobleaching, a laser-induced process that is also heralded by a visible change of the emission signal. The combination of these two activation and deactivation monitoring techniques allows to generate arrays with only one emitter per site. Our results deepen the knowledge of optically active deep defects in hBN and provides clear pathways towards the deterministic fabrication of top-down nanophotonic devices for applications to optical quantum information.

VII. METHODS

Sample fabrication

Our sample consists of a single crystal of high-pressure, high-temperature grown hBN [13] exfoliated on a SiO₂(300 nm)/Si substrate. After acetone and isopropanol cleaning, the sample is annealed at 1000 °C under 200 sccm nitrogen (N₂) flow during 1 h and left inside the oven during 3 h for cooling. This technique incentivizes the formation of UV emitters. The B centers are created by 3 kV irradiation and an electron current of I=0.01-0.1 nA in a commercial scanning electron microscope in high vacuum conditions ($P<10^{-4}$ Pa) at room temperature.

VIII. ACKNOWLEDGMENTS

This work is supported by the French Agence Nationale de la Recherche (ANR) under references ANR-21-CE47-0004. This work received government funding under France 2030 (QuanTEdu-France) with reference number ANR-22-CMAS-0001. The Authors acknowledge K. Watanabe and T. Taniguchi for providing hBN crystals, and thank J.-M. Chauveau and C. Vilar for fruitful discussions.

^[1] Aharonovich, I.; Englund, D.; Toth, M. Solid-State Single-Photon Emitters. *Nature Photon*. 2016, *10*, 631–641.

^[2] Bernien, H.; Hensen, B.; Pfaff, W. et al. Heralded entanglement between solid-state qubits separated by three metres. Nature 497, 86–90 (2013).

^[3] Azzam, S. I.; Parto, K.; Moody, G. Prospects and challenges of quantum emitters in 2D materials. Appl. Phys. Lett. 2021; 118 (24): 240502.

^[4] Tran, T. T.; Bray, K.; Ford, M. J.; Toth, M.; Aharonovich, I. Quantum emission from hexagonal boron nitride monolayers. *Nat. Nanotechnol.* 2016, 11, 37-41.

^[5] Martínez, L. J.; Pelini, T.; Waselowski, V.; Maze, J. R.; Gil, B.; Cassabois, G.; Jacques, V. Efficient Single Photon Emission

from a High-Purity Hexagonal Boron Nitride Crystal. *Phys. Rev. B* 2016, 94, 121405.

^[6] Fournier, C.; Roux, S.; Watanabe, K.; Taniguchi, T.; Buil, S.; Barjon, J.; Hermier, J.-P.; Delteil, A. Two-Photon Interference from a Quantum Emitter in Hexagonal Boron Nitride. *Phys. Rev. Appl.* 2023, *19*, L041003.

^[7] Gérard, D.; Buil, S.; Watanabe, K.; Taniguchi, T.; Hermier, J.-P.; Delteil, A. Resonance fluorescence and indistinguishable photons from a coherently driven B centre in hBN, arXiv:2506.16980 (2025).

^[8] Shevitski, B.; Gilbert, S. M.; Chen, C. T.; Kastl, C.; Barnard, E. S.; Wong, E.; Ogletree, D. F.; Watanabe, K.; Taniguchi, T.; Zettl, A.; Aloni, S. Blue-Light-Emitting Color Centers in High-

- Quality Hexagonal Boron Nitride. Phys. Rev. B 2019, 100, 155419.
- [9] Fournier, C.; Plaud, A.; Roux, S.; Pierret, A.; Rosticher, M.; Watanabe, K.; Taniguchi, T.; Buil, S.; Quélin, X.; Barjon, J.; Hermier, J.-P.; Delteil, A. Position-Controlled Quantum Emitters with Reproducible Emission Wavelength in Hexagonal Boron Nitride. *Nat. Commun.* 2021, 12, 3779.
- [10] Gale, A.; Li, C.; Chen, Y.; Watanabe, K.; Taniguchi, T.; Aharonovich, I.; Toth, M. Site-Specific Fabrication of Blue Quantum Emitters in Hexagonal Boron Nitride. ACS Photonics 2022, 9, 2170.
- [11] Gérard, D.; Rosticher, M.; Watanabe, K.; Taniguchi, T.; Barjon, J.; Buil, S.; Hermier, J.-P.; Delteil, A. Top-Down Integration of a hBN Quantum Emitter in a Monolithic Photonic Waveguide. Appl. Phys. Lett. 2023, 122, 264001.
- [12] Spencer, L.; Horder, J.; Kim, S.; Toth, M.; Aharonovich, I. Monolithic Integration of Single Quantum Emitters in hBN Bullseye Cavities. ACS Photon. 2023, 10, 4417.
- [13] Taniguchi, T.; Watanabe, K. Synthesis of High-Purity Boron Nitride Single Crystals Under High Pressure by Using Ba–BN Solvent. J. Cryst. Growth 2007, 303, 525-529.
- [14] Silly, M. G.; Jaffrennou, P.; Barjon, J.; Lauret, J.-S.; Ducastelle, F.; Loiseau, A.; Obraztsova, E.; Attal-Tretout, B.; Rosencher, E.; Luminescence Properties of Hexagonal Boron Nitride: Cathodoluminescence and Photoluminescence Spectroscopy Measurements. Phys. Rev. B 2007, 75 (8), 085205.
- [15] Museur, L.; Feldbach, E.; Kanaev, A. Defect-Related Photoluminescence of Hexagonal Boron Nitride. Phys. Rev. B: Condens. Matter Mater. Phys. 2008, 78 (15), 155204.
- [16] Bourrelier, R.; Meuret, S.; Tararan, A.; Stéphan, O.; Kociak, M.; Tizei, L. H. G.; Zobelli, A. Bright UV Single Photon Emission at Point Defects in h-BN. *Nano Lett.* 2016, 16, 4317
- [17] Schué, L.; Stenger, I.; Fossard, F.; Loiseau, A.; Barjon, J. Characterization Methods Dedicated to Nanometer-Thick hBN Layers. 2D Mater. 2017, 4 (1), 015028.
- [18] Onodera, M.; Watanabe, K.; Isayama, M.; Arai, M.; Masubuchi, S.; Moriya, R.; Taniguchi, T.; Machida, T. Carbon-Rich Domain in Hexagonal Boron Nitride: Carrier Mobility Degradation and Anomalous Bending of the Landau Fan Diagram in Adjacent Graphene. Nano Lett. 2019, 19 (10), 7282–7286.
- [19] Mackoit-Sinkevičienė, M.; Maciaszek, M.; Van de Walle, C. G.; Alkauskas, A. Carbon Dimer Defect as a Source of the 4.1 eV Luminescence in Hexagonal Boron Nitride. *Appl. Phys. Lett.* 2019, 115 (21), 212101.
- [20] Li, S.; Pershin, A.; Thiering, G.; Udvarhelyi, P.; Gali, A. Ultraviolet Quantum Emitters in Hexagonal Boron Nitride from Carbon Clusters. J. Phys. Chem. Lett. 2022, 13 (14), 3150–3157.
- [21] Plo, J.; Pershin A. et al. Isotope Substitution and Polytype Control for Point Defects Identification: The Case of the Ultraviolet Color Center in Hexagonal Boron Nitride, Phys. Rev. X 15, 021045
- [22] Roux, S.; Fournier, C.; Watanabe, K.; Taniguchi, T.; Hermier, J.-P.; Barjon, J.; Delteil, A. Cathodoluminescence Monitoring

- of Quantum Emitter Activation in Hexagonal Boron Nitride. *Appl. Phys. Lett.* 2022, *121*, 184002.
- [23] Nedić, S.; Yamamura, K.; Gale, A.; Aharonovich, I.; Toth, M. Electron Beam Restructuring of Quantum Emitters in Hexagonal Boron Nitride. Adv. Opt. Mater. 2024, 2400908.
- [24] Hou H.; Hua M. et al. Nanometer Resolution Structure-Emission Correlation of Individual Quantum Emitters via Enhanced Cathodoluminescence in Twisted Hexagonal Boron Nitride. Adv. Mater. 2025, e01611.
- [25] Zhigulin, I.; Horder, J.; Ivády, V.; White, S. J. U.; Gale, A.; Li, C.; Lobo, C. J.; Toth, M.; Aharonovich, I. Stark Effect of Blue Quantum Emitters in Hexagonal Boron Nitride. Phys. Rev. Appl. 2023, 19 (4), 044011.
- [26] Ganyecz, Á.; Babar, R.; Benedek, Z.; Aharonovich, I.; Barcza, G.; Ivády, V. First-Principles Theory of the Nitrogen Interstitial in hBN: A Plausible Model for the Blue Emitter. Nanoscale 2024, 16, 4125–4139.
- [27] Maciaszek M., Razinkovas L. Blue Quantum Emitter in Hexagonal Boron Nitride and a Carbon Chain Tetramer: a First-Principles Study. ACS Applied Nano Materials 2024 7 (16), 18979-18985.
- [28] Gale, A.; Kianinia, M.; Horder, J.; Tweedie, C.; Singhal, M.; Scognamiglio, D.; Qi, J.; Liu, K.; Verdi, C.; Aharonovich, I.; Toth, M. Quantum Emitters in Rhombohedral Boron Nitride. Adv. Opt. Mater. 2025, 13 (27), e00593.
- [29] Vuong, T. Q. P.; Cassabois, G.; Valvin, P.; Ouerghi, A.; Chassagneux, Y.; Voisin, C.; Gil, B. Phonon–Photon Mapping in a Color Center in Hexagonal Boron Nitride. Phys. Rev. Lett. 2016, 117 (9), 097402.
- [30] Bianco, F.; Pezzini, S.; Watanabe, K.; Taniguchi, T.; Fabbri, F. Scanning Electron Irradiation of Hexagonal Boron Nitride: An Efficient Procedure for Quenching Undesired Defects Emissions Monitored by In-Situ Room Temperature Cathodoluminescence. 2D Mater. 2025, 12 (2), 025026.
- [31] Gérard, D.; Pierret, A.; Fartas, H.; Berini, B.; Buil, S.; Hermier, J.-P.; Delteil, A. Quantum efficiency and vertical position of quantum emitters in hBN determined by Purcell effect in hybrid metal-dielectric planar photonic structures, ACS Photonics 11, 5188 (2024).
- [32] Hamdi, H.; Thiering, G.; Bodrog, Z.; Ivády, V.; Gali, A. Stone–Wales Defects in Hexagonal Boron Nitride as Ultraviolet Emitters. npj Comput. Mater. 2020, 6, 178.
- [33] Weston, L.; Wickramaratne, D.; Mackoit, M.; Alkauskas, A.; Van de Walle, C. G. Native Point Defects and Impurities in Hexagonal Boron Nitride. Phys. Rev. B 2018, 97, 214104.
- [34] Alem, N.; Erni, R.; Kisielowski, C.; Rossell, M. D.; Hartel, P.; Jiang, B.; Gannett, W.; Zettl, A. Vacancy Growth and Migration Dynamics in Atomically Thin Hexagonal Boron Nitride under Electron Beam Irradiation. Phys. Status Solidi RRL 2011, 5 (8), 295–297.
- [35] Zobelli, A.; Ewels, C. P.; Gloter, A.; Seifert, G. Vacancy Migration in Hexagonal Boron Nitride. Phys. Rev. B 2007, 75 (9), 094104.